

# Force and Moment Characterization of Flapping Wings for Micro Air Vehicle Application

Zaeem A. Khan, Graduate Student, Sunil K. Agrawal, Ph.D., Professor  
 Department of Mechanical Engineering  
 University of Delaware, Newark, DE 19716  
 agrawal@me.udel.edu

**Abstract**— This paper presents a method for investigating the unsteady aerodynamics of flapping wings for micro air vehicle application. For this purpose, a robotic flapper was designed and fabricated which can flap dynamically scaled wings in a desired kinematic pattern. An aerodynamic model and wing testing methodology was developed based on unsteady aerodynamic mechanisms. This model additionally accounts for the wing twisting. The experimental results show a good agreement with published data and the aerodynamic model compares well with the experimental results. The focus of the present work is on hovering flight, however, the methodology is general and can be extended to forward flight in future.

## I. INTRODUCTION

The creation of flapping wing micro air vehicles (FW-MAV) is a challenging problem. Flapping wing flight offers high maneuverability and the capability to hover as witnessed in insects and hummingbirds. These properties make FWMAVs suitable for micro air vehicle missions such as reconnaissance and surveillance.

As shown in Fig. 1, the aerodynamic module is fundamental to the design process of a FWMAV. The module takes the wing and body kinematics as inputs and gives the aerodynamic forces and torques. These are then used to compute the rigid body dynamics, navigation and control algorithms, and to perform design optimization. The aerodynamics of flapping wings is unsteady and a largely unexplored area. Due to the complexity of solving Navier-Stokes equation [2] for flow around flapping wings, experimental methods are widely used. Experimental investigation of fruit fly aerodynamics has been reported [6]. Flow visualization experiments using scaled hawkmoth wings were performed [5]. These experiments led to the discovery of unsteady aerodynamic mechanisms that are responsible for high lift in biological flying species.

In our work, we conduct experiments on flapping wings using a robotic flapper. However, our focus is the FWMAV aerodynamics and design. Therefore, we keep the wing kinematics to be very general and use a generic insect-like wing for testing. We have additionally taken into account the effects of wing twist along the span. The aerodynamic moments are also determined experimentally using a six-axis force torque sensor. Based on these results, we present a model which takes into account the unsteady effects. This model constitutes the aerodynamic module.

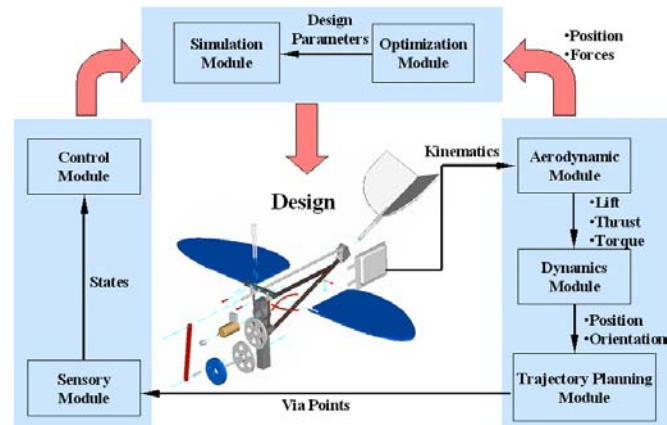


Fig. 1. The architecture of FW-MAV Design

## II. AERODYNAMIC MODEL

### A. Wing motion terminology

We consider the left wing of a typical insect. As shown in Fig. 2(A), the wing frame  $(x_w, y_w, z_w)$  can be described by three successive rotations with respect to frame  $(x_s, y_s, z_s)$  attached at the wing base. First, rotation about  $z_s$  axis by an angle  $\phi$ , next a rotation about the current  $x'$  axis by an angle  $\theta$  and finally rotation about the current  $y''$  axis by an angle  $\psi$ . Therefore, the wing position is given by the body sequence 3-1-2 rotation and by angles  $(\phi, \theta, \psi)$ .  $\phi$  is called the flap angle. The motion of the wing due to flap angle  $\phi$  is called the *flapping translational motion* as shown in Fig. 2(B). For a wing section located at a distance  $r$  from the flapping axis, the translational speed is given by  $\dot{\phi}r$ .  $\psi$  is the rotation or feather angle. The  $y_w$  axis attached to the wing is the feather axis. The rotation of the wing about the feather axis through an angle  $\psi$  is referred to as the *rotational motion*. Flapping wing typically rotates at the extremes of the stroke. The plane defined by  $(x_s, y_s)$  axes represents the *stroke plane*. The frame  $(x_s, y_s, z_s)$  is referred to as the *stroke plane frame*.  $\theta$  is the out of stroke plane or elevation angle. If  $\theta = 0$ , the motion is called planar flapping. In this paper, we will consider planar flapping.

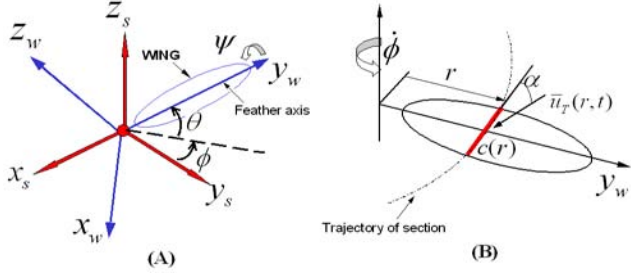


Fig. 2. (A) Wing angles ( $\phi, \theta, \psi$ ). (B) Translational motion

### B. Quasi-steady state analysis

The steady state force equation for flapping wing can be derived using the blade element method (BEM). The force on a section of wing at a distance  $r$  from the flapping axis is given by

$$dF_{steady} = \frac{\rho}{2} C_F(\alpha) |\bar{u}_T(r, t)|^2 c(r) dr, \quad (1)$$

where  $|\bar{u}_T(r, t)|$  is the translational speed of the section,  $C_F(\alpha)$  is the force coefficient of the section which is a function of the local angle of attack  $\alpha$  and  $c(r)dr$  is the area of the section.

Simplified models based on quasi-steady state assumption have been developed [10]. According to this assumption, the motion during flapping cycle is replaced by a series of static positions having instantaneous velocity and angle of attack [3]. The force is determined using Eq. (1) which is not a function of wing rotation and acceleration. It is only a function of the translational speed  $|\bar{u}_T(r, t)| = \dot{\phi}r$  of the section. The quasi-steady analysis underestimates the lift required to support an insect during hovering [3].

### C. Quasi-unsteady state analysis

Based on a study of different aerodynamic models [1], [7] and [9], we modify Eq. (1) as follows

$$dF_T = dF_{steady}(\dot{\phi}) + dF_{unsteady}(\dot{\phi}, \dot{\psi}, \ddot{\phi}, \ddot{\psi}), \quad (2)$$

where  $dF_T$  is the total force on the section,  $dF_{steady}$  is the steady state or translational force given by Eq. (1) and  $dF_{unsteady}$  is the unsteady force which is a function of wing rotation and acceleration. The current focus is to determine the mathematical form of  $dF_{unsteady}$ .

#### Leading edge vortex (LEV) Force

When a thin wing translates at a high angle of attack a vortex is created above the leading edge which increases the circulation and consequently the lift force significantly [2, 4]. It was also found that in revolving wings undergoing translational motion, the LEV remains attached and the resultant force due to LEV remains normal to the wing surface [4]. Based on this study, we conclude

that the force due to LEV ' $dF_{lev}$ ' acts normal to the wing surface and it is not a function of wing rotation and acceleration. Therefore, it can be modeled by steady-state Eq. (1) which can be thought of as a product of a function  $dF_1 = 1/2 \rho |\bar{u}_T(r, t)|^2 c(r) dr$  which captures the physics of  $dF_{steady} = dF_{lev}$  and a coefficient  $C_1(\alpha)$  that adjusts the magnitude. Since  $dF_{lev}$  is generated during the translational phase of wing motion, it can be referred to as translational force.

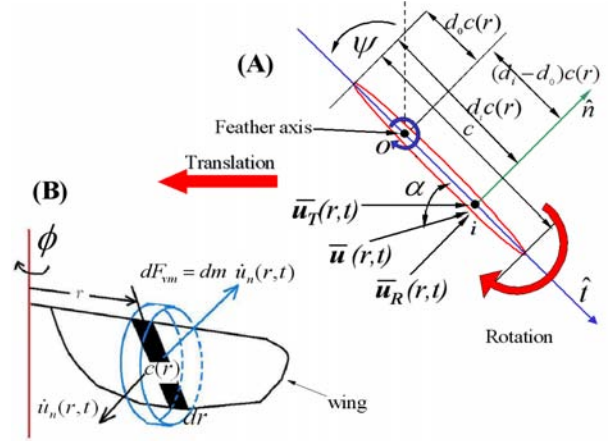


Fig. 3. (A) The combined rotational and translational/LEV effect on a wing section. (B) Virtual mass force acting at a section.

#### Rotational Force

If the wing rotates about the feather axis with an angular rate  $\dot{\psi}$ , a rotational circulation force is generated which can be modeled by selecting the flow velocity  $|\bar{u}_T(r, t)|$  in Eq. (1) at a location ' $i$ ' along the chord [9] as shown in Fig. 3(A). The total flow velocity  $\bar{u}(r, t)$  can be written as a vector sum of translational velocity  $\bar{u}_T(r, t)$  and rotational velocity  $\bar{u}_R(r, t)$ . The combined rotational and translational force is given by

$$dF_{lev+rot} = C_1(\alpha) \frac{\rho}{2} |\bar{u}(r, t)|^2 c(r) dr, \quad (3)$$

The coefficient of rotational force  $C_2$  appears as the non-dimensional parameter  $d_i - d_o(r)$  in the expression for  $|\bar{u}(r, t)|$  which can be adjusted to scale the rotational force. If the wing has only translation then Eq. (3) simplifies to Eq. (1) and we get the translational force only.

*Angle of attack ( $\alpha$ ):* The local or section angle of attack  $\alpha$  is given by

$$\alpha = \tan^{-1} \left[ \frac{u_n(r, t)}{u_t(r, t)} \right] \text{sgn}(u_t), \quad -\pi/2 < \alpha < \pi/2 \quad (4)$$

where  $u_n(r, t)$  and  $u_t(r, t)$  are the components of  $\bar{u}(r, t)$  normal and tangential to the chord.

### Virtual Mass force

As the wing accelerates, it moves along with it a mass of air, assumed to be contained in a cylinder with diameter equal to the chord [1], [3]. The acceleration of this mass of air shows up as a virtual mass force (see Fig. 3B) and can be written as

$$dF_{virtual\ mass} = C_3 \frac{\rho\pi}{4} \dot{u}_n(r, t) c(r)^2 dr = C_3 dF_3. \quad (5)$$

where  $\dot{u}_n(r, t)$  is the rate of change of normal velocity component at the mid-chord location in the wing frame and  $dm = \rho\pi c^2/4$  is the mass of air enclosed in a thin cylinder of width  $dr$  and a diameter equal to the chord  $c(r)$  at a distance  $r$  from the flapping axis. The coefficient  $C_3$  is included in order to adjust the magnitude while the function  $dF_3$  captures the physics of virtual mass effect.

### D. Total Force

We can write the total force on a section as a sum of Eq. (3) and Eq. (5)

$$dF_T = C_1 \frac{\rho}{2} |\bar{u}(r, t)|^2 c(r) dr + C_3 \frac{\rho\pi}{4} \dot{u}_n(r, t) c(r)^2 dr, \quad (6)$$

If we substitute the expressions for  $u_n(r, t)$  and  $\dot{u}_n(r, t)$  in Eq. (6), we get

$$dF_T = C_1 dF_1 + dF_2(C_1, C_2) + C_3 dF_3, \quad (7)$$

where  $C_1 dF_1$  is  $dF_{lev}$  and  $dF_2(C_1, C_2)$  and  $C_3 dF_3$  are the unsteady rotational and virtual mass forces respectively. Eq. (7) can be integrated for the entire wing. Therefore,  $F_T = C_1 F_1 + F_2(C_1, C_2) + C_3 F_3$ .

### E. Assumptions in the model

- Superposition of steady and unsteady aerodynamic effects holds.
- LEV force can be modeled by the steady-state aerodynamic equation.
- Chordwise-force due to skin friction is ignored based on experimental results [4].
- The total force  $dF_T$  acts normal to the chord and at the mid-chord location at every section throughout the flapping cycle.

## III. EXPERIMENTAL INVESTIGATION

### A. Robotic Flapper

In order to determine the coefficients  $C_1$ ,  $C_2$  and  $C_3$ , we conducted experimental investigation. For this purpose, a robotic flapper was designed and fabricated at the University of Delaware. It is shown in Fig. 4. The flapper is driven by three independent servo motors designed to give three degrees-of-freedom flapping motion, i.e.,  $\phi, \theta, \psi$ .

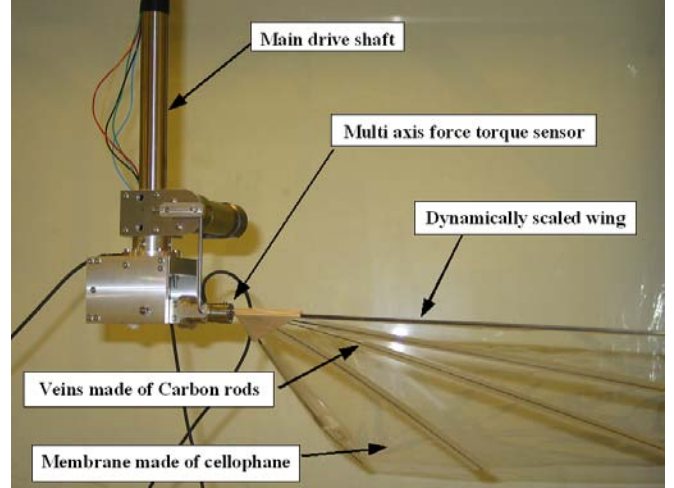


Fig. 4. Figure shows the robotic flapper designed and fabricated at University of Delaware. It is driven by three independent servo motors and can give 3-DOF flapping wing motion. A six-axis force torque sensor (Nano 17) from ATI industrial automation is mounted at the base of the wing.

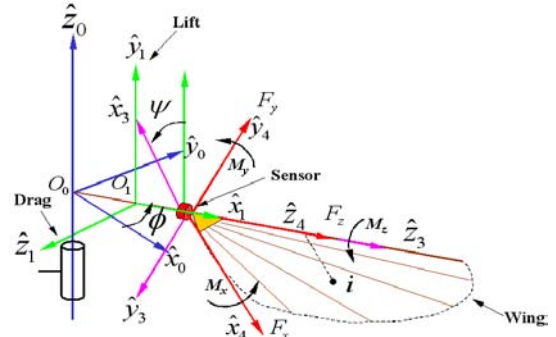


Fig. 5. Figure shows the sensor co-ordinate frame  $f_4$  and the positive direction of force and moment components ( $F_x, F_y, F_z, M_x, M_y, M_z$ ). The directions of lift and drag force are also identified.

### Flapper Kinematics

The flapper coordinate system is shown in Fig. 5. For the case of hovering flight, the body of FWMAV is assumed to be stationary with respect to the earth. The body frame  $f_o(x_0, y_0, z_0)$  is also the inertial frame. The rotation matrices between the frame  $f_1(x_1, y_1, z_1)$  and the wing frame  $f_3(x_3, y_3, z_3)$  and between the wing frame  $f_3$  and sensor frame  $f_4(x_4, y_4, z_4)$  are given by

$$R_1^3 = \begin{pmatrix} 0 & 0 & 1 \\ C_\psi & -S_\psi & 0 \\ S_\psi & C_\psi & 0 \end{pmatrix}, \quad R_3^4 = \begin{pmatrix} -1 & 0 & 0 \\ 0 & -1 & 0 \\ 0 & 0 & 1 \end{pmatrix}, \quad (8)$$

The lift and drag force is given by

$$\begin{pmatrix} 0 \\ Lift \\ Drag \end{pmatrix} = R_1^4 \begin{pmatrix} F_x \\ F_y \\ F_z \end{pmatrix}, \quad (9)$$

TABLE I  
WING GEOMETRY USED IN THE EXPERIMENT

section	spanwise location 'r'(m),	chord c(r)(m),	$d_o(r)\%$
1	0.105	0.270	0
2	0.155	0.287	0
3	0.205	0.284	0
4	0.255	0.271	0
5	0.305	0.261	0
6	0.355	0.254	0
7	0.405	0.236	0
8	0.455	0.212	0
9	0.505	0.180	-0.03
10	0.555	0.115	-0.27

where *Lift* and *Drag* are along  $\hat{y}_1$  and  $\hat{z}_1$  directions respectively and  $R_1^4 = R_3^3 R_3^4$ . The velocity and normal acceleration components are given by

$$|\bar{u}(r, t)|^2 = (\dot{\phi} r \sin \psi)^2 + (\dot{\phi} r \cos \psi + C_2 c(r) \dot{\psi})^2, \quad (10)$$

$$\dot{u}_n(r, t) = -(\ddot{\phi} r \cos \psi - \dot{\psi} \dot{\phi} \sin \psi + 0.5 c(r) \ddot{\psi}), \quad (11)$$

If we substitute  $|\bar{u}(r, t)|^2$  and  $\dot{u}_n(r, t)$  given by Eq. (10) and Eq. (11) into Eq. (6) and integrate, we get the total force  $F_T = C_1 F_1 + F_2(C_1, C_2) + C_3 F_3$  where

$$F_1 = \frac{\rho}{2} \dot{\phi}^2 \int_0^R r^2 c(r) dr \quad (12)$$

$$F_2 = \frac{\rho}{2} [2C_1 C_2 \dot{\psi} \dot{\phi} \cos \psi \int_0^R r c(r)^2 dr + C_2^2 \dot{\psi}^2 \int_0^R c(r)^3 dr] \quad (13)$$

$$F_3 = \frac{\rho \pi}{4} [-\ddot{\phi} \cos \psi \int_0^R r c(r)^2 dr + \dot{\psi} \dot{\phi} \sin \psi \int_0^R c(r)^2 dr - 0.5 \ddot{\psi} \int_0^R c(r)^3 dr] \quad (14)$$

### B. Flow similarity

To achieve flow similarity, the reduced frequency  $K$  along with Reynolds number  $Re$  and wing geometry should match for the prototype and experimental wing. For the case of hovering flapping flight, these are given by [4, 10]

$$Re = \frac{8\Phi R^2 f}{\nu \Lambda}, \quad K = \frac{\pi}{2\Phi \Lambda}. \quad (15)$$

where  $\nu$  is the kinematic viscosity,  $R$  is the wing length,  $\Phi$  is the flapping amplitude,  $f$  is the flapping frequency in cycles/sec and  $\Lambda$  is the wing aspect ratio. We selected an  $Re$  range for FWMAV design to be 12,000-25,000 based on hummingbird. The scaled wing geometry used in the experiment is given in Table I.

### C. Force and Moment in sensor frame

From observations of wing during the experiment, we found that the wing deforms due to aerodynamic loads. Both spanwise bending and twist were present. As a first approximation, we ignore the spanwise bending. We model

twist by assuming a linear variation from root to the tip of the wing. The twist  $\delta\psi_i$  at the  $i^{th}$  section is given by

$$\delta\psi_i = \beta \frac{r_i - r_o}{R - r_o}, \quad \beta = K_\beta [u_n(r_m, t)]^2 \text{sgn}(u_n). \quad (16)$$

where  $r_i$  is the location of the section,  $r_o$  is the distance between the root chord and the flapping axis and  $r_m$  is the location of a section at the mid-span, for instance, section 5 in Table I.  $\beta$  is the magnitude of twist proportional to the normal velocity  $u_n(r_m, t)$  computed at  $r_m$ . The normal velocity is squared to give the same effect as aerodynamic force. The magnitude of the twist is visually matched with the experiment by varying the value of the coefficient  $K_\beta$ . Based on the assumption that the total force at the  $i^{th}$  section is normal to the chord, we can transform this force into the sensor frame as follows:

$$\begin{pmatrix} dF_x^i \\ dF_y^i \\ dF_z^i \end{pmatrix} = \begin{pmatrix} C_{\delta\psi_i} & -S_{\delta\psi_i} & 0 \\ S_{\delta\psi_i} & C_{\delta\psi_i} & 0 \\ 0 & 0 & 1 \end{pmatrix} \begin{pmatrix} 0 \\ dF_T^i \\ 0 \end{pmatrix}, \quad (17)$$

The moments in the sensor frame can be computed as follows:

$$dM_x^i = -r_i dF_y^i, \quad dM_y^i = r_i dF_x^i, \quad (18)$$

$$dM_z^i = [0.5 - d_o(r_i)] c(r_i) dF_T^i, \quad (19)$$

where 0.5 gives the mid-chord location of  $dF_T^i$  based on our assumption. The forces and moments can be summed in the sensor frame

$$F_x = \sum_{i=1}^N dF_x^i, \quad F_y = \sum_{i=1}^N dF_y^i, \quad F_z = \sum_{i=1}^N dF_z^i = 0 \quad (20)$$

$$M_x = \sum_{i=1}^N dM_x^i, \quad M_y = \sum_{i=1}^N dM_y^i, \quad M_z = \sum_{i=1}^N dM_z^i \quad (21)$$

where the  $F_z$  component of sensor force is ignored since it is in the spanwise direction. Therefore,

$$F_T = \sqrt{F_x^2 + F_y^2}. \quad (22)$$

## IV. DETERMINATION OF COEFFICIENTS

### A. Determination of $C_1$

In order to determine  $C_1$ , we select the flapping kinematics such that the functions  $F_2$  and  $F_3$  become zero at some point in the flapping cycle but  $F_1$  remains non-zero. This means  $\dot{\phi} \neq 0$ , while  $\dot{\psi} = \ddot{\phi} = \ddot{\psi} = 0$ . We selected the following kinematic pattern

$$\phi(t) = \Phi \sin(\omega t), \quad \psi(t) = -\Psi \cos(\omega t), \quad (23)$$

where  $\Phi$  and  $\Psi$  are flap and rotational amplitudes respectively. This pattern gives  $\dot{\psi} = 0$  and maximum values of

TABLE II  
TESTING SCHEME

Flap Amplitude $\Phi$ (deg).	$Re$	$K$
46	12,404	0.332
63	17,000	0.2477
74.5	20,000	0.2095

TABLE III  
ANGLE OF ATTACK AT MID-STROKE, ( $\phi = 0^0$ )

s.no.	Rotational Amplitude $\Psi$ (deg).	$\alpha$ (deg)
*	90.0	0.0
1	75.0	15.0
2	64.0	26.0
3	52.4	37.6
4	41.2	48.8
5	30.0	60.0
6	19.0	71.0
7	8.0	82.0
8	0.0	90.0

$\dot{\phi}$  and  $\ddot{\psi}$  at the mid-stroke position, i.e., at  $\phi = 0$ . The term involving  $\ddot{\psi}$  in  $F_3$  gives the rotational virtual mass effect which is small in comparison to the translational virtual mass effect and we ignore it in subsequent analysis. Therefore,  $F_2$  and  $F_3$  become zero and  $F_{lev} = C_1 F_1$  is non-zero at the mid-stroke. Therefore, the sensor measures  $F_T = F_{lev}$  and

$$C_1 = \frac{F_T}{F_1} = \frac{F_{lev}}{1/2\rho\dot{\phi}^2\int_0^R r^2 c(r)dr}, \quad \text{at } \phi = 0, \quad (24)$$

#### Procedure

Three different values of flap amplitude  $\Phi$  were chosen as shown in Table II along with values of  $Re$  and  $K$ . For each flap amplitude, the rotational amplitude  $\Psi$  and eight corresponding  $\alpha$  from 0 to  $90^\circ$  were chosen at the mid-stroke position, as shown in Table III. Experiment was not conducted at  $\alpha = 0^\circ$  and we assumed  $C_1(0) = 0$ . This is because normal force is zero on a symmetric flat plate at  $\alpha = 0$ . The chordwise friction force is ignored in our model. In all, 24 kinematic patterns were tested.

The plot of  $C_1$  against  $\alpha$  in Fig. 6 shows that the flap amplitude has little effect on the slope ( $dC_1/d\alpha$ ). Fig. 6 also shows a linear relationship between  $C_1$  and  $\alpha$  which can be approximated as  $C_1(\alpha) = \frac{7}{\pi}|\alpha|$ .

#### B. Determination of $C_2$

$C_1$  and  $C_2$  occur implicitly in  $F_2$ . Therefore, the best way to determine  $C_2$  is to adjust it until the model matches with the experimental results. The value of  $C_2$  is based on  $d_i$ . We found that  $d_i = 0.75$  gives best results.

#### C. Determination of $C_3$

If we modify the kinematic pattern given by Eq. (23) by taking  $\Psi = 0^0$ , then  $F_2$  becomes zero for the entire cycle while  $F_1$  becomes zero at the ends of the stroke,

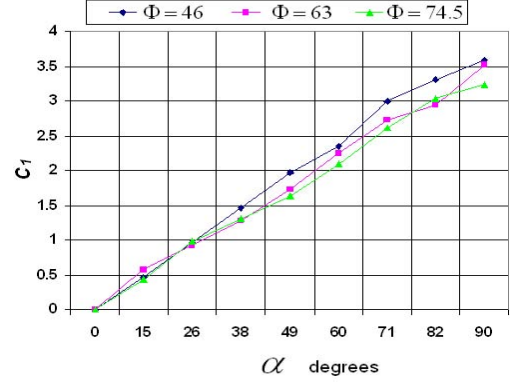


Fig. 6. Coefficient of LEV/translational force  $C_1$  Vs  $\bar{\alpha}$

i.e., at  $\phi = \phi_{max}$  and  $\dot{\phi} = 0$ . However,  $F_3$  is maximum there since  $\dot{\phi}$  is maximum. Therefore, the total force  $F_T$ , measured by the sensor at the ends of the stroke is due to virtual mass effect.

$$C_3 = \frac{F_T}{F_3} = \frac{F_{virtual\ mass}}{F_3}, \quad \text{at } \phi = \phi_{max}. \quad (25)$$

The value of  $C_3$  was found to vary between 0.5 and 1.0 for all 24 kinematic patterns.

#### V. COMPARISON OF EXPERIMENTAL RESULTS

In order to compare the experimental results with published data, we determine the coefficient of lift and drag at the mid-stroke. These are given by

$$C_L = \frac{Lift}{F_1}, \quad C_D = \frac{Drag}{F_1} \quad (26)$$

where *lift* and *drag* force is computed from Eq. (9). Eq. (26) is applicable since  $C_L$  and  $C_D$  are the decomposition of  $C_1$ . The polar plot in Fig. 7 shows high values of  $C_L$  and  $C_D$  and compares well with the published data [4, 8].

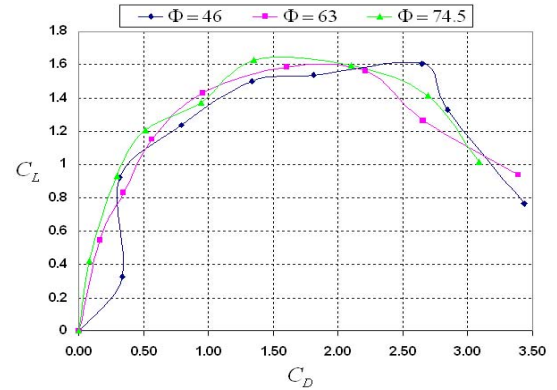


Fig. 7. Lift and drag polar plot for three stroke amplitudes, i.e.,  $\Phi = 46^\circ, 63^\circ, 74.5^\circ$ . These coefficients are computed at the mid-stroke position during the flapping cycle similar to the determination of  $C_1$ .

## VI. COMPARISON OF EXPERIMENTAL RESULTS WITH AERODYNAMIC MODEL

The coefficients  $C_1$ ,  $C_2$  and  $C_3$  will now be used in the aerodynamic model and comparison will be made with the experimental data. To compare the model with the experiment, we select two patterns having rotational amplitudes of  $\Psi = 75^\circ$  and  $\Psi = 0^\circ$  (entries 1 and 8 in Table III). In both cases, the flap amplitude is  $\Phi = 46^\circ$ . These represent the extreme cases. If the model compares well with the experimental data for these two cases, we expect good comparison for the patterns in between.

### A. Comparison of $F_y$ component of aerodynamic force

Fig. 8 shows the  $F_y$  component of aerodynamic force in the sensor frame for the two kinematic patterns. Fig. 8(A), (C) are the plots of individual aerodynamic mechanisms  $C_1F_1$ ,  $F_2$ ,  $C_3F_3$  which are components of the total force transformed in the sensor  $F_y$  direction for half cycle. Fig. 8(B), (D) shows how the individual aerodynamic mechanisms contribute to the total force which compares well with the experimental results.

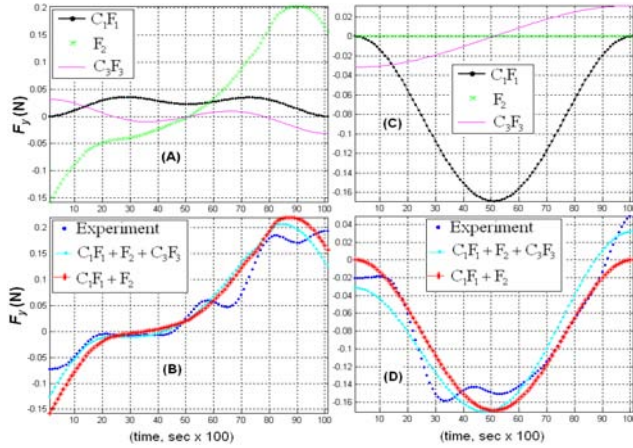


Fig. 8. Comparison of  $F_y$  component of total aerodynamic force  $F_T = C_1F_1 + F_2(C_1, C_2) + C_3F_3$ . (A) and (B) shows the comparison for the pattern having amplitudes  $\Phi = 46^\circ$ ,  $\Psi = 74.9^\circ$ , (C) and (D) shows the comparison for the pattern having amplitudes  $\Phi = 46^\circ$ ,  $\Psi = 0^\circ$ .

For the pattern in Fig. 8(A) and (B), the rotational force  $F_2$  dominates as far as magnitude is concerned. This shows that the quasi-steady aerodynamic force given by  $C_1F_1$ , is inadequate for modeling flapping wing aerodynamics when wing rotation is present. The virtual mass force  $C_3F_3$  is maximum at the ends of the stroke and adjusts the total force at the ends as shown in Fig. 8(D). However, its contribution is small compared to translational and rotational effects.

### B. Comparison of $F_x$ component of aerodynamic force

The match with the experimental data is less accurate in the case of  $F_x$  component. This is due to the approximate

match of twist  $\delta\psi$  with the actual wing in terms of both the spanwise distribution as well as variation during the cycle. We found this typical behavior in all the 24 kinematic patterns.

### C. Comparison of aerodynamic moments

The  $M_x$  and  $M_z$  components show a good match with the experimental data. The accuracy of  $M_x$  component indicates that the model accurately distributes the  $F_y$  component along the span. Similarly, the accuracy of  $M_z$  component indicates that our assumption of mid-chord location of force  $dF_T$  at every section is valid. The comparison of  $M_y$  component is approximate due to the fact that it is dependent on  $F_x$  component which compared approximately with the experiment. This behavior of moments was found to be consistent in all 24 kinematic patterns.

## VII. CONCLUSION

This paper presents a methodology for the experimental determination of steady and unsteady aerodynamic force coefficients based on the principle of dynamic similarity. These coefficients are used in the quasi-unsteady aerodynamic model which additionally takes into account the wing twist due to aerodynamic loads.

The purpose of this research was to develop the aerodynamic module which is an essential part of FWMAV system modeling and design as shown in Fig. 1. Based on the results, we conclude that the model can be used in the aerodynamic module for the determination of aerodynamic force and moment components. However for any given wing shape, the coefficients must be determined using the robotic flapper. This procedure can also be used to optimize wing geometry and wing kinematics.

## REFERENCES

- [1] DELaurier, J. D., "An Aerodynamic Model for Flapping-Wing Flight". *Aeronautical Journal*, Vol. 97, No. 964 April 1993, pp.125-130 .
- [2] Hao Liu, Ellington, C. P. Kawachi Keiji, Van Den Berg and Willmott A.P.; " A Computational Fluid Dynamic Study of Hawkmoth Hovering". *Journal of Experimental Biology*, 201, 461-477 (1998) .
- [3] Ellington, C. P. (1984a). " The aerodynamics of hovering insect flight. I-V". *Phil. Trans. Royal Society of London B* 305, 115.
- [4] Usherwood, J. R. and Ellington, C. P. (2002). " The aerodynamics of revolving wings. I and II". *J. Exp. Biol.* 205, 1547-1564.
- [5] Willmott A. P., Ellington, C. P. and Adrian L.R. Thomas (1997). " Flow visualization and unsteady aerodynamics in the flight of the hawkmoth, *Manduca sexta*." *Phil. Trans. R. Soc. Lond. B* (1997) 352, 303-316.
- [6] Dickinson, M.H, Lehmann, F.O., Sane, S.P (1997). " Wing Rotation and the Aerodynamic Basis of Insect Flight."
- [7] Sane, S.P, and Dickinson, M.H (2001). "The aerodynamic effects of wing rotation and a revised quasi-steady model of flapping flight" *Journal of Experimental Biology*, 205, 1087-1096 (2002)
- [8] Sane, S.P (2003). "The aerodynamics of insect flight" *Journal of Experimental Biology*, 206, 4191-4208 (2003)
- [9] Walker, J. A., (2002). "Rotational lift: something different or more of the same?". *Journal of Experimental Biology*, 205, 3783-3792 (2002) .
- [10] Robert Dudley. "The biomechanics of insect flight, form, function and evolution."